

STRUCTURE NOTE

Crystal structure of homoisocitrate dehydrogenase from *Schizosaccharomyces pombe*

Stacie L. Bulfer, Jenna M. Hendershot, and Raymond C. Trievel^{*}

Department of Biological Chemistry, University of Michigan, Ann Arbor, Michigan 48109

Key words: X-ray crystallography; amino acid metabolism; lysine biosynthesis; β -hydroxyacid oxidative decarboxylase.

INTRODUCTION

Lysine biosynthesis in fungi, euglena, and certain archaebacteria occurs through the α -aminoadipate pathway.¹ Enzymes in the first steps of this pathway have been proposed as potential targets for the development of antifungal therapies, as they are absent in animals but are conserved in several pathogenic fungi species, including *Candida*, *Cryptococcus*, and *Aspergillus*.² One potential antifungal target in the α -aminoadipate pathway is the third enzyme in the pathway, homoisocitrate dehydrogenase (HICDH), which catalyzes the divalent metal-dependent conversion of homoisocitrate to 2-oxoadipate (2-OA) using nicotinamide adenine dinucleotide (NAD⁺) as a cofactor.¹

HICDH belongs to a family of β -hydroxyacid oxidative decarboxylases that includes malate dehydrogenase, tartrate dehydrogenase, 6-phosphogluconate dehydrogenase, isocitrate dehydrogenase (ICDH), and 3-isopropylmalate dehydrogenase (IPMDH). ICDH and IPMDH are well-characterized enzymes that catalyze the decarboxylation of isocitrate to yield 2-oxoglutarate (2-OG) in the citric acid cycle and the conversion of 3-isopropylmalate to 2-oxoisovalerate in the leucine biosynthetic pathway, respectively.³ Recent structural and biochemical studies of HICDH reveal that this enzyme shares sequence, structural, and mechanistic homology with ICDH and IPMDH.^{3–7} To date, the only published structures of HICDH are from the archaebacteria *Thermus thermophilus* (TtHICDH).^{6,8} Fungal HICDHs diverge from TtHICDH in several aspects, including their thermal stability, oligomerization state, and substrate specificity, thus warranting further characterization. To gain insights into these differences, we determined crystal structures of

a fungal *Schizosaccharomyces pombe* HICDH (SpHICDH) as an apoenzyme and as a binary complex with the additive tripeptide glycyl-glycyl-glycine (GGG) to 1.55 Å and 1.85 Å resolution, respectively. Finally, a comparison of the SpHICDH and TtHICDH structures reveal differences in their active sites that help explain the variations in their respective substrate specificities.

MATERIALS AND METHODS

Cloning, expression, and purification

Full length HICDH encoded by the *Lys12*⁺ gene in *S. pombe* was amplified from the genomic clone SPAC31G5.04 (Sanger Institute) and was subcloned into a modified pET15b N-terminal 6xHIS-tag expression vector (Novagen) that contains a tobacco etch virus protease cleavage site. The enzyme was overexpressed in the Rosetta 2 strain (EMD Biosciences) by induction with 0.1 mM isopropyl β -D-1-thiogalactopyranoside at 22°C

Additional Supporting Information may be found in the online version of this article.

Grant sponsor: United States Department of Energy, Basic Energy Sciences, Office of Science; Grant number: DE-AC02-06CH11357; Grant sponsor: Michigan Economic Development Corporation; Grant sponsor: the Michigan Technology Tri-Corridor; Grant number: 085P1000817; Grant sponsor: NIH CBTP Training grant; Grant number: 5T32GM008353; Grant sponsors: Predoctoral Fellowship (U.M. Rackham Graduate School) and a Graduate Student Research Grant.

Stacie L. Bulfer's current address is Department of Pharmaceutical Chemistry, University of California, San Francisco, San Francisco, CA 94158, USA.

^{*}Correspondence to: Raymond Trievel, Department of Biological Chemistry, University of Michigan, 5301 Medical Science Research Building III, 1150 West Medical Center Drive, SPC 5606, Ann Arbor, MI 48109.

E-mail: rtrievel@umich.edu

Received 27 September 2011; Accepted 17 October 2011

Published online 24 October 2011 in Wiley Online Library (wileyonlinelibrary.com). DOI: 10.1002/prot.23231

for 16 h. Cells were resuspended in 50 mM sodium phosphate, pH 7.0, 500 mM NaCl, 5 mM β -mercaptoethanol and were lysed with lysozyme followed by sonication. Soluble enzyme was purified on a Talon (Clontech) Co(II) column, and the 6xHIS tag was removed by incubating with tobacco etch virus protease during dialysis overnight against 50 mM sodium phosphate, pH 7.0, 150 mM NaCl, and 5 mM β -mercaptoethanol. The His-tagged protease was removed by passing the sample over a second Talon Co(II) column. SpHICDH was further purified by gel filtration via isocratic elution with 50 mM sodium phosphate, pH 7.0, 150 mM NaCl, and 1 mM tris(2-carboxyethyl)phosphine on a Superdex 200 column (GE healthcare). The protein was concentrated to 100–120 mg/mL (A_{280} , $\epsilon = 17,420$) and stored at -80°C .

Crystallization, data collection, and structure determination

Crystals of SpHICDH were initially obtained by vapor diffusion in a condition with 0.2M lithium acetate and 20% (w/v) PEG 3350. The Additive Screen HT (Hampton Research) was used to determine that the addition of 30 mM GGG improved crystal quality. Optimization was performed at 20°C in hanging drops composed of 1.5 μL of 25 mg/mL SpHICDH, 1.5 mM 2-OA, 60 mM GGG as an additive and 1.5 μL crystallization solution (0.22M lithium acetate and 18% (w/v) PEG 3350). SpHICDH was also crystallized by hanging drop vapor diffusion using 1 μL of 15–24 mg/mL SpHICDH, 2 mM MgCl_2 , 6.6 mM 2-OA, and 2 mM NAD^+ in 1 μL 0.1–0.25M lithium acetate, 12–16% PEG 3350. Crystals were cryoprotected in their crystallization solution supplemented with 20% glycerol and subsequently frozen in liquid nitrogen. Diffraction data were collected at LS-CAT, beamline 21ID-G at the Advanced Photon Source (Argonne National Labs), and data sets were integrated and scaled using HKL2000⁹ (Table I). A model of SpHICDH was generated in Chainsaw¹⁰ from the sequence alignment of SpHICDH and TtHICDH and the coordinates of the TtHICDH structure (PDB 1X0L),⁶ which was subsequently used as a search model for molecular replacement in MOLREP.¹¹ The model of SpHICDH bound to GGG was built in Coot¹² and refined in REFMAC¹³ using TLS refinement.¹⁴ This structure was used as a model for molecular replacement for SpHICDH apoenzyme crystallized in the presence of MgCl_2 , 2-OA, and NAD^+ , which was built and refined as described for the SpHICDH-GGG complex. The final models were validated using Molprobity¹⁵ (Table I). Root mean square deviations (RMSDs) were calculated for C α atoms using SSM Superpose in Coot.¹² A simulated annealing omit map of GGG was generated in CNS¹⁶, and structural figures were created using MacPyMOL (The PyMOL Molecular Graphics System, Schrödinger, LLC.)

Table I

Data Collection and Refinement Statistics

	SpHICDH (apoenzyme)	SpHICDH (GGG complex)
Data collection		
Beamline	21-ID-G	21-ID-G
Space group	P21	P21
Cell dimensions		
a, b, c, (Å)	52.85, 94.45, 76.08	53.24, 92.86, 75.47
β ($^\circ$)	106.6	106.7
Wavelength (Å)	0.97856	0.97856
Resolution (Å) ^a	25.0–1.55 (1.61–1.55)	20.0–1.85 (1.89–1.85)
R_{merge} (%) ^b	5.5 (45.9)	7.2 (41.5)
$I/\sigma I$	30.2 (2.9)	22.1 (2.7)
Total reflections	713,906	380,206
Unique reflections	103,345	60,681
Redundancy	6.9 (4.3)	6.3 (3.9)
Completeness (%)	99.3 (94.2)	99.5 (94.7)
Refinement		
Resolution range (Å)	24.86–1.55	19.70–1.85
No. of reflections	97,599	56,698
No. of atoms	6084	5761
Protein atoms	5524	5371
Ligand/Glycerol	–/60	26/24
Water atoms	500	340
$R_{\text{work}}/R_{\text{free}}^c$	18.8/21.5	19.3/23.0
Average B-factors (Å ²)		
Overall	22.1	26.5
Protein	22.2	26.7
Ligand/Glycerol	–/24.6	43.8/32.6
Water	20.9	21.5
RMSDs		
Bond length (Å)	0.012	0.014
Bond angles ($^\circ$)	1.409	1.413
MolProbity score ^d	1.32	1.49
Percentile ^e	96 th	95 th
Ramachandran favored (%)	97.3	97.2
Ramachandran allowed (%)	2.7	2.8
Ramachandran outliers (%)	0	0

^aValues in parentheses are for the highest-resolution shell.

^b $R_{\text{merge}} = \sum_{hkl} \sum_j |I_j - I| / \sum_{hkl} \sum_j I_j$ where I is the mean intensity of reflection hkl .

^c $R_{\text{work}} = \sum_{hkl} \|F_o| - |F_c|\| / \sum_{hkl} |F_o|$; $R_{\text{free}} = 5.1\%$ of the total reflections.

^d $0.42574 \times \log(1 + \text{clashscore}) + 0.32996 \times \log(1 + \max(0, \text{pctRotOut} - 1)) + 0.24979 \times \log(1 + \max(0, 100 - \text{pctRamaFavored} - 2)) + 0.5$

^eFor structures with a resolutions ± 0.25 Å of the resolution of each SpHICDH structure. 100th percentile is the best; 0th percentile is the worst.

RESULTS AND DISCUSSION

Overall structure of SpHICDH

The crystal structures of SpHICDH apoenzyme and complex with GGG were determined by molecular replacement to 1.55 Å and 1.85 Å, respectively (Table I). The quaternary structure of SpHICDH consists of domain-swapped monomers [Fig. 1(A)] with density observed for residues 5–360 and 4–360 of each monomer in the apoenzyme and residues 5–362 of monomer A and 5–53 and 57–359 of monomer B in the GGG-bound complex. Each SpHICDH monomer is composed of a large domain (residues 1–101 and 266–362), a small domain (residues 102–129 and 156–265), both of mixed α/β topology, and a clasp domain¹⁷ forming an antipar-

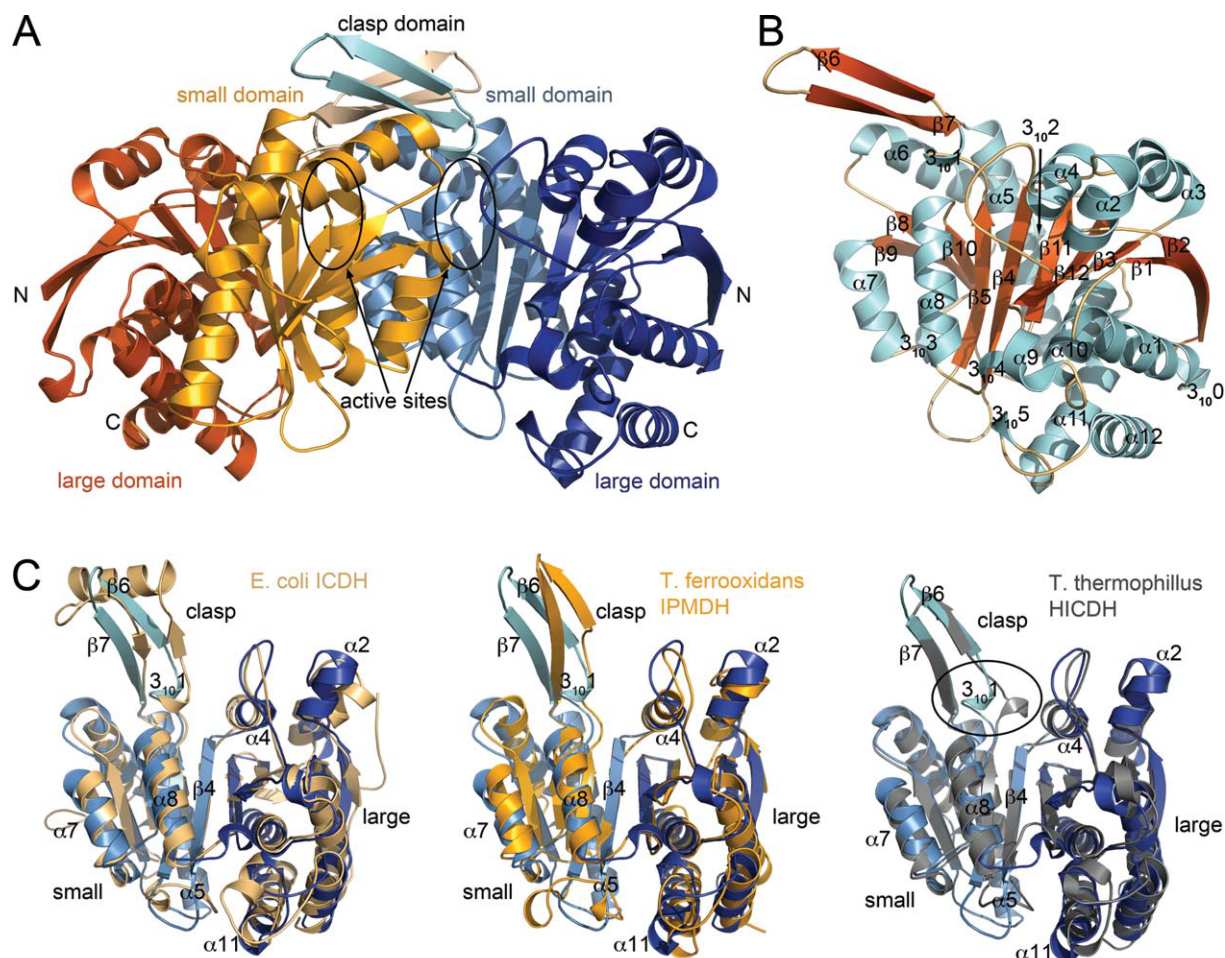


Figure 1

Crystal structure of SpHICDH (A) Ribbon diagram of a homodimer of SpHICDH with the large domain, small domain, and clasp domain of monomer A depicted in dark blue, light blue, and cyan, and of monomer B in dark orange, orange, and light orange, respectively. (B) Cartoon representation of the secondary structure of a monomer of SpHICDH with secondary structure elements labeled. (C) Ribbon diagram illustrating the superimposition of a monomer of SpHICDH [colored as described for monomer A in (A)] with those of EcICDH (PDB ID 1AI2, light orange), TfIPMDH (PDB entry 1A05, orange), and TtHICDH (PDB code 1X0L, gray). Rearrangement of the 3_{10} -helix between the SpHICDH and TtHICDH apoenzyme structures is circled.

allel β -sheet at the dimer interface (residues 130–156) [Fig. 1(A)]. The secondary structure of a monomer of SpHICDH adopts a modified Rossmann fold¹⁷ with 10 β -strands (β 1– β 5 and β 8– β 12) creating a mixed parallel and antiparallel β -sheet [Fig. 1(B)]. The remaining two β -strands (β 6– β 7) compose the clasp domain, which interacts with the adjacent monomer. Additional interactions at the dimer interface are predominantly mediated through the formation of a four-helix bundle between α 7 and α 8 from both monomers. This fold is homologous to other β -hydroxyacid oxidative decarboxylases including ICDHs (RMSDs 1.77 Å and 2.68 Å for PDB entries 1AI2 and 2QFV, respectively),^{18,19} IPMDHs (RMSDs 1.92 Å and 1.84 Å for PDB codes 1IPD and 1A05, respectively),^{20,21} and TtHICDH (RMSD 1.23 Å for PDB entry 1X0L).⁶

A structural comparison of SpHICDH with *Escherichia coli* ICDH (EcICDH) in a complex with isocitrate and NADPH,¹⁸ *Thiobacillus ferrooxidans* IPMDH (TfIPMDH) bound to isopropylmalate,²⁰ and TtHICDH⁶ illustrates similarities and differences among these enzymes [Fig. 1(C)]. Each of these enzymes adopts a closed conformation. The closed and open forms of these enzymes refer to the width of the NADH binding pocket, which is located in a cleft between the large and small domains below the active site [Fig. 1(A)]. For example, the EcICDH apoenzyme has been crystallized in the open and closed states, whereas substrate-bound EcICDH adopts a closed form, which is a result of a $\sim 16^\circ$ rotation of the large domain relative to the small domain that narrows the NADH binding cleft^{17,22}. The major difference between SpHICDH and other β -hydroxyacid

oxidative decarboxylases is the conformation of the clasp domain and the loop region following $\beta 4$. The 3_{10} -helix preceding the clasp also differs in its orientation between SpHICDH and TtHICDH apoenzyme (discussed below).

Active site of SpHICDH

The active site of SpHICDH is located in a cleft between the small and large domains of one monomer and also contains residues from the small domain of the neighboring monomer. [Fig. 1(A)]. Although 2-OA, NAD^+ , and Mg(II) were included in the crystallization condition, the ligands and metal ion were not observed in the electron density maps. Despite their absence, the apoenzyme's active site adopts a conformation homologous to the closed state EcICDH bound to isocitrate and NAD^+ ,¹⁸ *Saccharomyces cerevisiae* mitochondrial NADP-dependent ICDH (ScICDH) in a complex with isocitrate,¹⁹ and TfIPMDH bound to isopropylmalate.²⁰ Similarly, the TtHICDH apoenzyme also displays a closed state⁶ [Fig. 1(C)], suggesting that HICDH may not undergo an extensive active site conformational change as observed for IPMDH^{23,24} and ICDH enzymes.^{17,19,22} Alternatively, the crystallization conditions for the HICDH enzymes may simply force the enzyme into a closed state. Additional structures of the HICDH apoenzyme and complexes with substrates are needed to resolve this question.

The residues in the active site responsible for substrate binding and catalysis have been identified through homology with ICDH and IPMDH and by biochemical characterization of *S. cerevisiae* HICDH (SchICDH).³ A lysine-tyrosine pair composed of Lys-196' and Tyr-133 in SpHICDH (the prime (') denotes a residue in the adjacent monomer) have been implicated in the acid-base catalyzed reaction that converts homoisocitrate to 2-OA, based on kinetic studies of SchICDH [Fig. 2(A)].⁵ Additionally, three conserved aspartate residues (Asp232', Asp256, and Asp260) have been proposed to coordinate the divalent metal ion necessary for catalysis.⁶ Because SpHICDH adopts a closed conformation in the absence of substrates, its structure can be superimposed with that of an EcICDH-isocitrate complex²⁵ to gain insight into HICDH substrate recognition. Homoisocitrate is predicted to bind in a similar orientation as isocitrate, with its C1 carboxylate group and 2-hydroxyl groups coordinated to the active site metal ion. Three structurally conserved arginine residues (Arg97, Arg107, and Arg126) further stabilize the substrate through interactions with its C1 and C6 carboxylate groups [Fig. 2(A)]. To visualize the binding position of the second substrate, NAD^+ , a product complex of HICDH bound to 2-OA, NADH, and Mg(II) was modeled by aligning the active site residues to that of a product complex of mitochondrial ScICDH bound to NADPH and 2-OG¹⁹ [Fig 2(B)]. The modeled NADH binds in the active site cleft, adjacent to the product 2-OA, and is flanked by $\alpha 9$ and the loop

between $\beta 3$ and $\alpha 4$ of one monomer and $\alpha 7$ of the adjacent monomer [Figs. 1(B) and 2(B)]. The modeled NADH fits well into the active site cleft of SpHICDH; however, there is a clash between the ribose hydroxyl groups of the nicotinamide mononucleotide of NADH and Ser81 located in the $\beta 3$ - $\alpha 4$ loop of the protein, suggesting that a conformational change of this loop is required for coenzyme binding. In summary, the structural alignments illustrate that the active site residues of SpHICDH responsible for substrate binding and catalysis are conserved with the residues in other β -hydroxyacid oxidative decarboxylases.

Unexpectedly, we observed that the tripeptide additive GGG binds in the active site of SpHICDH. Two conserved arginine residues (Arg97 and Arg126), which are proposed to interact with homoisocitrate, form contacts with GGG through a network of direct and water-mediated hydrogen bonds [Fig. 2(C)]. The tripeptide is further stabilized by hydrogen bonding to the backbone atoms of residues Ser85, Val87, and Gly89, which are located in the loop between $\beta 3$ and $\alpha 4$. Additional hydrogen bonds occur between the α -amine group of GGG and Glu285 and Pro286. Together, these interactions orient the GGG tripeptide into a similar location as the modeled NADH and 2-OA products [Supporting Information Fig. S1]. Specifically, the backbone carbonyl of the second glycine is nearly superimposable with the modeled nitrogen in the ring of the nicotinamide moiety of NADH. Additionally, the C-terminal carboxylate of GGG is positioned between the amide nitrogen in the nicotinamide group of NADH and the C1 carboxylate of 2-OA, respectively.

Comparison of SpHICDH to TtHICDH

A comparison of the SpHICDH and TtHICDH structures reveals some key differences between the fungal and archaeal enzymes. First, the two enzymes exhibit distinct oligomerization states. SpHICDH eluted as a homodimer in size exclusion chromatography (data not shown) and crystallized in the same oligomerization state (Table I). In contrast, TtHICDH functions as a homotetramer, with the clasp domain of two dimers forming hydrophobic intersubunit interactions.^{6,7} This tetramerization state is presumably unique to archaeal HICHDs and may enhance the thermostability of the enzyme, as a mutation that disrupts tetramerization exhibits a lower thermal inactivation temperature.⁶ Moreover, the active site conformation differs between SpHICDH and TtHICDH apoenzyme despite their homologous structures [Figs. 1(C) and 2(D)]. In TtHICDH, the active site adopts a nonproductive conformation in which Tyr125 is flipped out of the active site cleft [Fig. 2(D)]. This observation lead Miyazaki *et al.* to speculate that either substrate binding is coupled to a conformational change in the active site or the TtHICDH structure represents a non-physiologically relevant structure, possibly induced by the

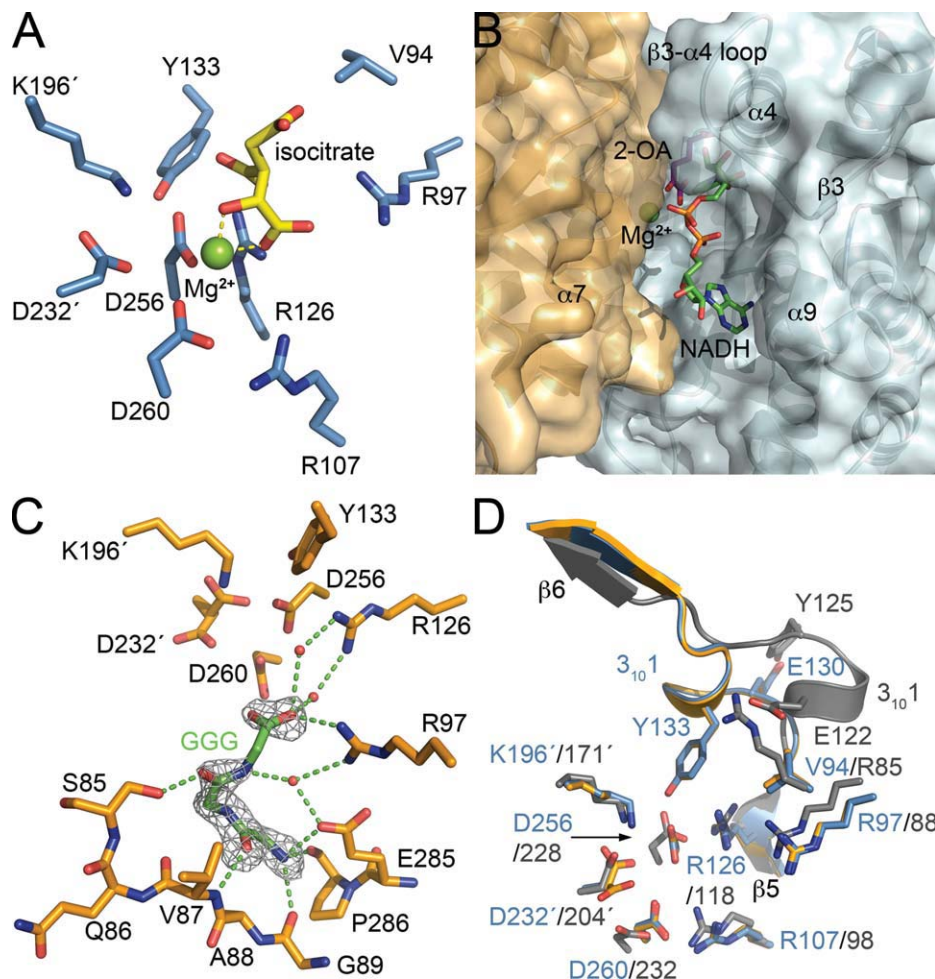


Figure 2

Active site of SpHICDH (A) Stick diagram of the active site of apo-SpHICDH with isocitrate and Mg(II) modeled from a superimposition with isocitrate dehydrogenase (PDB ID 5ICD). Isocitrate is modeled in stick configuration with yellow carbon atoms and the Mg(II) ion is shown as a green sphere. (B) A model of the product complex of SpHICDH. A surface representation of SpHICDH monomer A (orange) and monomer B (blue) illustrates the NAD⁺ binding cleft. The NADH and 2-OA products were modeled by aligning apo-SpHICDH with a product complex of ScICDH bound to NADPH and 2-OG (PDB code 2QFX). The Mg(II) ion is modeled as a green sphere, and 2-OA and NADH are illustrated with violet and green carbon atoms, respectively. (C) Stick diagram of the active site of SpHICDH bound to a GGG peptide (green carbons). Electron density of the $F_o - F_c$ simulated annealing omit map contoured to 2.0σ around the GGG peptide is shown in gray. Water molecules and hydrogen bonds are shown as red spheres and green dashes, respectively. (D) Overlay of the active site of apo-SpHICDH (blue), GGG-bound SpHICDH (orange), and TtHICDH (gray). Residues in SpHICDH and TtHICDH are labeled in blue and gray, respectively.

low pH of the crystallization condition.⁶ Conversely, in SpHICDH, the corresponding tyrosine (Tyr133) is oriented in a catalytically competent conformation due to a shift of the 3_{10} helix toward $\beta 6$ and $\beta 7$ of the clasp domain. In a recent study, the structure of TtHICDH in complex with a designed inhibitor is reported.⁸ Similar to SpHICDH, the catalytic tyrosine (Tyr125) is flipped inward and interacts with the inhibitor, indicating that it is important for catalysis, and possibly substrate binding. These findings suggest that the SpHICDH active site adopts a conformation that is conducive to substrate binding, whereas the nonproductive configuration observed in the TtHICDH apoenzyme structure may be a consequence of

the crystallization condition. Further structural studies of HICDH substrate and product complexes are needed to ascertain the extent of the conformational changes that occur in the active site during ligand binding.

In addition to variations in their oligomerization state and active site conformation, the substrate specificities of the fungal and archaeal HICDHs also differ. TtHICDH utilizes both isocitrate and homoisocitrate as substrates, whereas yeast HICDHs display greater specificity for homoisocitrate versus isocitrate.^{4,7,26} Mutagenesis studies in TtHICDH determined that substrate specificity is governed by a key active site residue, Arg85 in TtHICDH or Val94 in SpHICDH, which occupy the same position

in their active sites [Fig. 2(D)].⁷ This observation is particularly interesting in that the structurally equivalent residue in ICDHs is also a valine. ICDH specificity towards its preferred substrate is instead governed by serine and asparagine residues (Ser113 and Asn115 in EcICDH), which form interactions with the C5 carboxylate of isocitrate [Supporting Information Fig. S2].^{25,27} The serine residue is conserved in HICDHs, but the asparagine is an isoleucine in yeast and archaeal HICDHs. Based on an SpHICDH-isocitrate model [Fig. 2(A)], Val94 may form van der Waals interactions to isocitrate, whereas in TtHICDH the corresponding Arg85 could potentially hydrogen bond to C5 carboxylate of isocitrate, equivalent to the interaction of the asparagine residue in ICDHs. Thus, this model offers a potential explanation for the ability of TtHICDH to efficiently oxidize both citrate and homocitrate. In summary, these observations suggest potential routes to exploit structural variations between the active sites of fungal and other β -hydroxyacid oxidative decarboxylases to design HICDH-specific inhibitors.

ACKNOWLEDGMENTS

The authors thank the Sanger Institute for providing the genomic DNA for SpHICDH and Spencer Anderson for assistance in X-ray data collection. They also thank Jim Hurley and Paul Del Rizzo for reading the manuscript and providing useful comments. Structures were deposited in the RCSB Protein Data Bank with accession codes 3TY3 and 3TY4 for the GGG-complex and apoenzyme, respectively.

REFERENCES

- Xu H, Andi B, Qian J, West AH, Cook PF. The alpha-aminoadipate pathway for lysine biosynthesis in fungi. *Cell Biochem Biophys* 2006;46:43–64.
- Garrad RC, Bhattacharjee JK. Lysine biosynthesis in selected pathogenic fungi: characterization of lysine auxotrophs and the cloned *LYS1* gene of *Candida albicans*. *J Bacteriol* 1992;174:7379–7384.
- Aktas DF, Cook PF. A lysine-tyrosine pair carries out acid-base chemistry in the metal ion-dependent pyridine dinucleotide-linked beta-hydroxyacid oxidative decarboxylases. *Biochemistry* 2009;48:3565–3577.
- Lin Y, Alguindigue SS, Volkman J, Nicholas KM, West AH, Cook PF. Complete kinetic mechanism of homoisocitrate dehydrogenase from *Saccharomyces cerevisiae*. *Biochemistry* 2007;46:890–898.
- Lin Y, West AH, Cook PF. Site-directed mutagenesis as a probe of the acid-base catalytic mechanism of homoisocitrate dehydrogenase from *Saccharomyces cerevisiae*. *Biochemistry* 2009;48:7305–7312.
- Miyazaki J, Asada K, Fushinobu S, Kuzuyama T, Nishiyama M. Crystal structure of tetrameric homoisocitrate dehydrogenase from an extreme thermophile, *Thermus thermophilus*: involvement of hydrophobic dimer-dimer interaction in extremely high thermotolerance. *J Bacteriol* 2005;187:6779–6788.
- Miyazaki J, Kobashi N, Nishiyama M, Yamane H. Characterization of homoisocitrate dehydrogenase involved in lysine biosynthesis of an extremely thermophilic bacterium, *Thermus thermophilus* HB27, and evolutionary implication of beta-decarboxylating dehydrogenase. *J Biol Chem* 2003;278:1864–1871.
- Nango E, Yamamoto T, Kumasaka T, Eguchi T. Structure of *Thermus thermophilus* homoisocitrate dehydrogenase in complex with a designed inhibitor. *J Biochem*, in press; PMID: 21813504.
- Otwinowski Z, Minor W. Processing of X-ray diffraction data collected in oscillation mode. *Methods Enzymol* 1997;276:307–326.
- Stein N. CHAINSAW: a program for mutating pdb files used as templates in molecular replacement. *J Appl Crystallogr* 2008;41:641–643.
- Vagin AA, Teplyakov A. MOLREP: an automated program for molecular replacement. *J Appl Crystallogr* 1997;30:1022–1025.
- Emsley P, Cowtan K. Coot: model-building tools for molecular graphics. *Acta Crystallogr Sect D: Biol Crystallogr* 2004;60:2126–2132.
- Murshudov GN, Vagin AA, Dodson EJ. Refinement of macromolecular structures by the maximum-likelihood method. *Acta Crystallogr Sect D: Biol Crystallogr* 1997;53:240–255.
- Winn MD, Murshudov GN, Papiz MZ. Macromolecular TLS refinement in REFMAC at moderate resolutions. *Methods Enzymol* 2003;374:300–321.
- Davis IW, Leaver-Fay A, Chen VB, Block JN, Kapral GJ, Wang X, Murray LW, Arendall WB, 3rd, Snoeyink J, Richardson JS, Richardson DC. MolProbity: all-atom contacts and structure validation for proteins and nucleic acids. *Nucleic Acids Res* 2007;35:375–383.
- Brunger AT, Adams PD, Clore GM, DeLano WL, Gros P, Grosse-Kunstleve RW, Jiang JS, Kuszewski J, Nilges M, Pannu NS, Read RJ, Rice LM, Simonson T, Warren GL. Crystallography & NMR system: a new software suite for macromolecular structure determination. *Acta Crystallogr Sect D: Biol Crystallogr* 1998;54:905–921.
- Hurley JH, Thorsness PE, Ramalingam V, Helmers NH, Koshland DE, Jr, Stroud RM. Structure of a bacterial enzyme regulated by phosphorylation, isocitrate dehydrogenase. *Proc Natl Acad Sci USA* 1989;86:8635–8639.
- Mesecar AD, Stoddard BL, Koshland DE, Jr. Orbital steering in the catalytic power of enzymes: small structural changes with large catalytic consequences. *Science* 1997;277:202–206.
- Peng Y, Zhong C, Huang W, Ding J. Structural studies of *Saccharomyces cerevisiae* mitochondrial NADP-dependent isocitrate dehydrogenase in different enzymatic states reveal substantial conformational changes during the catalytic reaction. *Protein Sci* 2008;17:1542–1554.
- Imada K, Inagaki K, Matsunami H, Kawaguchi H, Tanaka H, Tanaka N, Namba K. Structure of 3-isopropylmalate dehydrogenase in complex with 3-isopropylmalate at 2.0 Å resolution: the role of Glu88 in the unique substrate-recognition mechanism. *Structure* 1998;6:971–982.
- Imada K, Sato M, Tanaka N, Katsube Y, Matsuura Y, Oshima T. Three-dimensional structure of a highly thermostable enzyme, 3-isopropylmalate dehydrogenase of *Thermus thermophilus* at 2.2 Å resolution. *J Mol Biol* 1991;222:725–738.
- Finer-Moore J, Tsutakawa SE, Cherbavaz DR, LaPorte DC, Koshland DE, Jr, Stroud RM. Access to phosphorylation in isocitrate dehydrogenase may occur by domain shifting. *Biochemistry* 1997;36:13890–13896.
- Hurley JH, Dean AM. Structure of 3-isopropylmalate dehydrogenase in complex with NAD⁺: ligand-induced loop closing and mechanism for cofactor specificity. *Structure* 1994;2:1007–1016.
- Kadono S, Sakurai M, Moriyama H, Sato M, Hayashi Y, Oshima T, Tanaka N. Ligand-induced changes in the conformation of 3-isopropylmalate dehydrogenase from *Thermus thermophilus*. *J Biochem* 1995;118:745–752.
- Hurley JH, Dean AM, Sohl JL, Koshland DE, Jr, Stroud RM. Regulation of an enzyme by phosphorylation at the active site. *Science* 1990;249:1012–1016.
- Chen R, Jeong SS. Functional prediction: identification of protein orthologs and paralogs. *Protein Sci* 2000;9:2344–2353.
- Yaoi T, Miyazaki K, Oshima T. Substrate recognition of isocitrate dehydrogenase and 3-isopropylmalate dehydrogenase from *Thermus thermophilus* HB8. *J Biochem* 1997;121:77–81.